Surface & Coatings Technology 236 (2013) 262–268

Contents lists available at ScienceDirect

Surface & Coatings Technology

journal homepage: www.elsevier.com/locate/surfcoat

Electrochemical impedance spectroscopy and indentation studies of pure and composite electroless Ni–P coatings

Mohammad Islam [a,*], Muhammad Rizwan Azhar [b], Narjes Fredj [c], T. David Burleigh [c]

[a] Center of Excellence for Research in Engineering Materials (CEREM), Advanced Manufacturing Institute, King Saud University, P. O. Box 800, Riyadh 11421, Saudi Arabia
[b] Department of Chemical Engineering, College of Engineering, King Saud University, Riyadh 11421, Saudi Arabia
[c] Materials and Metallurgical Engineering Department, New Mexico Institute of Mining and Technology, Socorro, NM 87801, USA

ARTICLE INFO

Article history:
Received 5 July 2013
Accepted in revised form 27 September 2013
Available online 8 October 2013

Keywords:
Electroless nickel
Composite coatings
Nanostructures
EIS
Microhardness

ABSTRACT

Electroless Ni–P coatings offer excellent corrosion and wear resistance and ability to withstand acidic and salt solutions. Medium and high phosphorus Ni–P coatings were produced using plating baths with 10 g/L or 25 g/L of sodium hypophosphite as reducing agent (RA) with composition of the resulting deposits to be 91.5 Ni: 8.5 P and 87.6 Ni: 12.4 P, respectively. From field-emission scanning electron microscope (FE-SEM) examination, the deposit morphology was found to change from nodular with surface porosity and cracks to dense, smooth upon increasing the RA content. Addition of nanostructures such as nanoparticles of alumina (Al_2O_3) or silicon carbide (SiC) or multi-walled carbon nanotubes (CNT) into Ni–P matrix, at low loading levels, was investigated for their effect on corrosion resistance and hardness of Ni–P–Al_2O_3, Ni–P–SiC and Ni–P–CNT composite coatings. Electrochemical impedance spectroscopy (EIS) studies in 4 wt.% NaCl solution revealed 91.5 Ni: 8.5 P coating to offer much superior corrosion resistance than 87.6 Ni: 12.4 P coating even after immersion for 42 days. Among all composite coatings, however, Ni–P–Al_2O_3 produced from 1.0 g/L Al_2O_3 in plating solution exhibits higher impedance values at low and intermediate frequencies. Nyquist plots for different frequencies were analyzed for comparison between different composite coatings. Microhardness tests indicate higher hardness value of 8.46 GPa for Ni–P–SiC coating as compared to 7.42 GPa for pure Ni–P coating.

1. Introduction

Unlike electroplating, electroless process involves synthesis of alloy coatings without an external current. Among a wide variety of coating types, Ni–P coatings are most commonly used due to their excellent mechanical, electrical, and magnetic properties. Generally, medium- and high-P coatings offer excellent protection against corrosion with reasonably high levels of hardness and wear resistance and can be a suitable alternative to industrial electroplated nickel and hard chromium coatings that suffer from disadvantages of non-uniform thickness, low ductility and susceptibility to hydrogen embrittlement [1]. Ni–P coatings with high P content are ideally poised for use in the applications involving high wear and corrosion resistance. The density of Ni–P films decreases significantly with increasing P content as compared to that of pure nickel.

When particles of a different composition and phase are dispersed into the plating bath solution, co-deposition of Ni–P as a matrix and dispersed particles as reinforcing phase will occur during the electroless plating, resulting in formation of composite coatings. While Ni–P coating is deposited via autocatalytic action of first the substrate and then the initial deposit layer, the particles are transported from the solution to the vicinity of the surface through convective-diffusion although there are other modes of particle incorporation as well, namely adsorption, mechanical entrapment, and electrophoresis. The intended role of such added nanostructures may be a dramatic change in deposit morphology and reduction/enhancement of cathode surface area depending on their electrical conductivity value [2]. Pure and composite Ni–P coatings with homogeneously dispersed second phase particles, having excellent wear and corrosion resistance, hold strong potential for use in petrochemical, oil and gas, food processing, and cutting tool industries [3]. The current state of research on development of electroless alloy and composite coatings from the perspective of difficult substrates and waste treatment is reviewed recently [4].

For uniform, homogeneous distribution of the particles in the composite coating, agitation mechanism such as bath circulation, magnetic stirring, or ultrasound is employed. In case of ultrafine particles, an appropriate surfactant like hexadecyltrimethyl ammonium bromide, sodium dodecyl sulfate, or cetyltrimethylamine bromide can also be used to avoid agglomeration due to surface charges and sedimentation [5,6]. Incorporation of hard particles such as Al_2O_3 [7–9], B_4C [10], BN [11], SiC [12–15], SiO_2 [16], TiO_2 [17,18] or ZrO_2 [19] into pure Ni–P coatings enhances hardness, despite their adverse effect on wear properties due to abrasive nature of added particles. Incorporation of ~20 vol.% SiC

* Corresponding author. Tel.: +966 11 467 0760 (work); fax: +966 92 51 9085 5002.
E-mail addresses: Mohammad.islam@gmail.com, miqureshi@ksu.edu.sa (M. Islam), rizwanazharr@yahoo.com (M.R. Azhar), nfredj@nmt.edu (N. Fredj), burleigh@nmt.edu (T.D. Burleigh).

0257-8972/$ – see front matter © 2013 Elsevier B.V. All rights reserved.
http://dx.doi.org/10.1016/j.surfcoat.2013.09.057

particles, 0.5 to 1.0 μm in size, was found to increase Vickers hardness to a maximum value of 875 with an associated increase in the friction coefficient from ~0.16 to 0.41 due to abrasive properties of SiC particles [12]. On the other hand, the inclusion of carbon nanotubes (CNTs) into Ni–P matrix coating was reported to prevent the rough contact between metallic surfaces by sliding or rolling between the surfaces [20]. Another study reported that addition of CNTs up to ~11.2 vol.% led to a gradual decrease in wear rate [6]. In fact, CNT addition can reduce the wear rate by one-third of that for pure Ni–P coatings presumably due to build-up of a protective oxide transfer layer within the wear scar, thus improving wear resistance. Improvement in corrosion resistance can be attributed to relatively low chemical reactivity and pore-filling action of the CNTs resulting in more compact films [21].

The published literature, in most cases, aims at addition of large amounts of the particles within Ni–P coating matrix. If particle size is at the nanoscale, its use in high quantities necessitates addition of an appropriate dispersing agent or surfactant to the plating bath making the bath chemistry more complicated. Also, there is a scarcity of reports on EIS studies of pure and nanocomposite Ni–P coatings for long immersion times. In our work, medium- and high-phosphorus Ni–P coatings were initially produced by varying the amount of sodium hypophosphite as reducing agent and compared for their microstructure, composition, corrosion resistance and microhardness. After that, nanocomposite coatings containing small amounts of second phase nanostructures (Al_2O_3, SiC or carbon nanotubes) were produced from precursor solutions without using any surfactant and their beneficial effects on hardness and corrosion properties were explored. Electrochemical impedance spectroscopy studies of both pure and nanocomposite Ni–P coatings were carried out in 4 wt.% NaCl solution for a maximum immersion period of four weeks. Indentation experiments were performed to compare microhardness values of pure and some of the composite coatings.

2. Materials and methods

All the chemicals for making aqueous electroless plating bath, namely nickel chloride ($NiCl_2$), sodium hypophosphite (NaH_2PO_2), sodium succinate ($C_4H_4Na_2O_4$), and sodium chloride (NaCl) were procured from Sigma-Aldrich with analytical purity of 99% or higher. For Ni–P–X composite coatings, alumina (Al_2O_3, 99.9%) and silicon carbide (SiC, 99%) nanoparticles as well as multi-walled carbon nanotubes (CNT, 95%) were obtained from Nanoshell LLC, USA and used without any further pre-treatment.

Using copper coupons 25 × 25 × 3 mm in size as substrates, the surfaces were prepared by grinding on SiC emery paper to 1200 grit size and polishing with 1 μm diamond paste. Following that, the substrates were cleaned in an ultrasonic bath and rinsed with deionized water. After drying, the deposition was carried out through immersion of the substrate into plating bath in presence of magnetic stirring. For pure Ni–P coatings, two plating bath compositions with 10 or 25 g/L of NaH_2PO_2 as reducing agent (RA) were made. For composite coatings, an aqueous suspension of the desired nanostructure (Al_2O_3, SiC or CNT) was initially prepared followed by mixing with nickel electroless plating bath. The dispersion of nanostructures in the bath and their homogeneous distribution in the matrix was ensured by means of ultrasonic treatment before mixing the two solutions and continuous stirring during coating deposition and growth. Also, a pre-coat of the pure Ni–P was applied over the copper substrate to promote high deposition rate of the composite coatings. The net weight gain was determined by taking into consideration the samples weights before and after coating deposition. The identification scheme and synthesis conditions of pure and composite Ni–P coatings are given in Table 1.

The surface morphology and elemental composition of the coatings were determined using field-emission scanning electron microscope (FE-SEM) from JEOL (JSM7600F). The microscope was operated at 15 kV with working distance (WD) of 4.5 mm for good resolution at high magnification whereas for energy dispersive spectrum (EDS) analysis, the value of WD was increased to 10 mm in order to secure reasonably high counts per second. X-ray diffraction (XRD) patterns were obtained using an X-ray diffractometer from Bruker (D8 DISCOVER) at operating voltage and current of 20 kV and 5 mA, respectively. For 2θ values in the range 30–100°, the step size and dwell time were maintained at 0.2° and 3 s, respectively.

Table 1
Electroless deposition conditions and identification scheme for pure and composite Ni–P samples.

S. no.	ID	Composition	Pre-coat	Synthesis conditions	Weight gain, mg
1.	S_1	Ni–P	×	90 °C, 60 min	15.5
2.	S_4	Ni–P	×	90 °C, 60 min	11.9
3.	S_1A_1	Ni–P–Al_2O_3	S_1	90 °C, 2 h; 0.25 g/L Al_2O_3 NP	16.3
4.	S_1A_2	Ni–P–Al_2O_3	S_1	90 °C, 2 h; 1.0 g/L Al_2O_3 NP	10.4
5.	S_1C_1	Ni–P–SiC	S_1	90 °C, 2 h; 0.25 g/L SiC NP	24.2
6.	S_4C_2	Ni–P–SiC	S_4	90 °C, 2 h; 1.0 g/L SiC NP	14.1
7.	S_1N_1	Ni–P–CNT	S_1	90 °C, 2 h; 0.25 g/L CNT	9.6

Electrochemical impedance spectroscopy (EIS) studies were performed to compare the corrosion resistance of pure and composite coatings in synthetic seawater containing 4 wt.% (wt%) NaCl solution. All the specimens were prepared by making an electrical contact of the specimen with a copper wire using a conductive silver paint. The samples were then embedded in an epoxy solution with hardener for curing and drying and were subsequently placed in sealed Erlenmeyer flasks containing 250 mL of 4 wt.% NaCl solution. The flasks were eventually sealed with Parafilm to avoid solution evaporation over time. The three-electrode method was employed with the coated sample, a saturated calomel electrode (SCE) and a platinum wire as working electrode, the reference electrode and the counter electrode, respectively. The electrodes were connected to a Princeton Applied Research Parstat 2263 potentiostat running PowerSuite corrosion analysis software. The EIS measurements were performed at the open circuit potential (OCP) values from 1 kHz to 10 mHz with 5 mV (rms) of amplitude per second and five points per decade. The surface area of the samples was between 0.34 and 4 cm^2. The EIS data was obtained after immersion in 4 wt.% NaCl solution for up to 22 days.

The hardness of the coatings was measured using nanoindentation system from Micro Materials (NanoTest Vantage) at a maximum applied load of 100 mN. For this purpose, each sample was mounted on the stub using a small amount of cyanoacrylate adhesive and at least 10 tests were performed using a Berkovich indenter.

3. Results and discussion

3.1. Coating structure and composition

The effect of sodium hypophosphite as reducing agent (RA) on coating morphology was investigated as manifested by low and high magnification FE-SEM micrographs, shown in Fig. 1. The high magnification view of S_1 coating surface (Fig. 1b) reveals presence of nodular structure with surface porosity and cracks. As the amount of RA is increased from 10 to 25 g/L (sample S_4), the degree of surface roughness decreases with no continuous cracks between spherical granules. In that case, fine pores with size of the order of 50 nm or less are seen predominantly at the boundaries between deposited granules (Fig. 1d). Since reducing agent is a source of electrons for reduction of Ni^{2+} and P^{3+} ions at the substrate (or growing coating surface), an increase in the RA content in the plating bath enhances the overall coating deposition rate thus leading to lower degree of surface roughness and porosity in the coating. Beside surface morphology, there is also an accompanying increase in P content in the coating from 8.5 to 12.4 wt.%, as noticed during EDS studies. Thus, changes in the plating bath composition strongly influence the P content in the resulting deposit and the coatings characteristics.

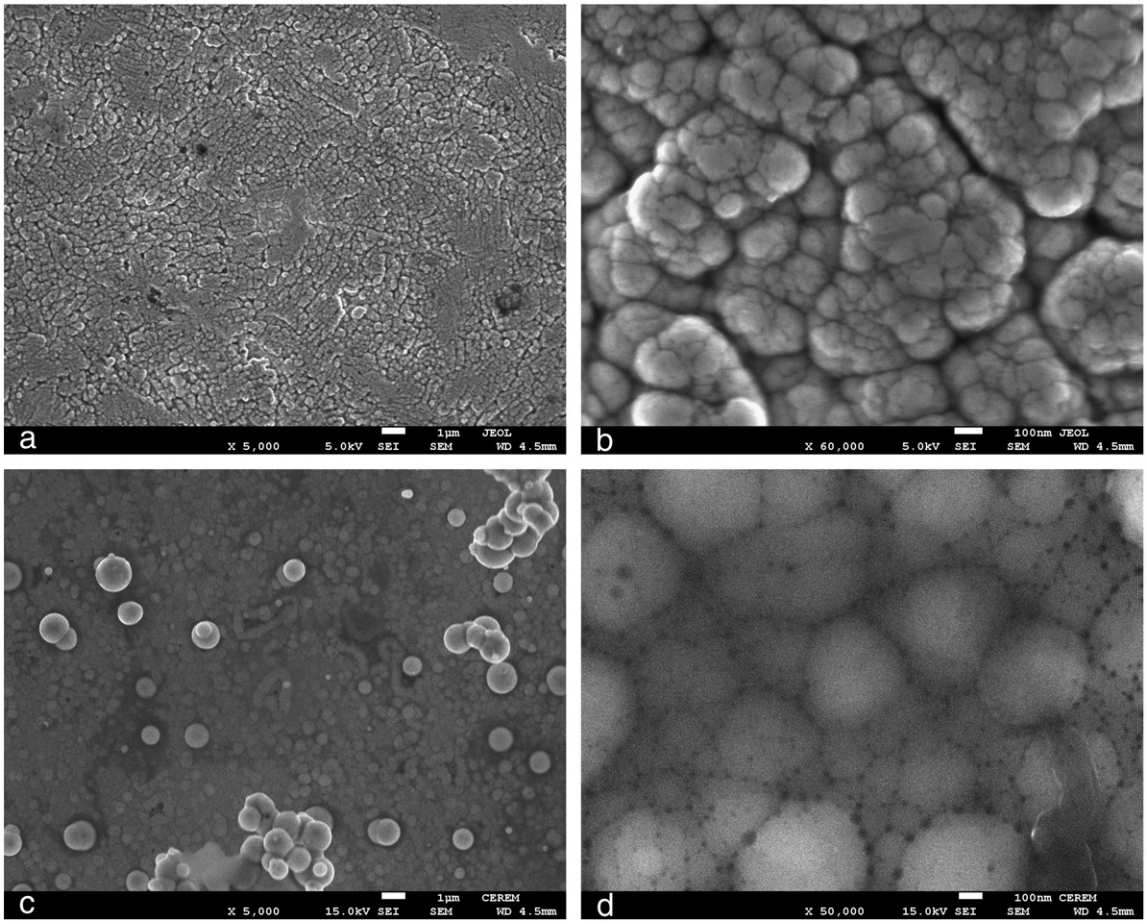

Fig. 1. Low and high magnification FE-SEM images of Ni–P coating surfaces: (a, b) S_1 and (c, d) S4.

The X-ray diffraction patterns of the pure Ni–P coating (S_1) and composite coatings incorporating Al_2O_3, SiC or multi-walled nanostructures are presented in Fig. 2. For pure and nanocomposite S_1 composition, the diffraction patterns indicate formation of crystalline deposits with distinct peaks characteristic of different Ni_xP_y phases. It is possible that co-deposition of P atoms along with Ni is more homogeneous due to solution chemistry, continuous stirring and island growth mode all of which have been reported to favor crystalline nature of the deposit [22,23]. This finding is also in agreement with our earlier work on electroless Ni–P coatings prepared under slightly different conditions [24,25]. Comparison of XRD patterns suggests promotion of $Ni_{2.55}P$ phase formation as a result of addition of these nanoparticles since the relative intensity of this peak is very small in the Ni–P coating. Overall, all the coatings are crystalline and no signature peak for Al_2O_3, SiC or CNT appeared presumably due to small amounts of these nanostructures used.

The nanoparticles (Al_2O_3, SiC) and CNT were characterized for their size and morphologies and the composite coatings were assessed for distribution of these nanostructures in the Ni–P matrix. Fig. 3 shows high magnification micrographs of Al_2O_3 and CNT and composite coating surfaces. The Al_2O_3 nanoparticles are found to be spherical with average size of ~15 nm (Fig. 3a), whereas carbon nanotubes are few microns in length with an outer diameter of ~60 nm (Fig. 3c) along with other carbonaceous forms in the as-received CNTs. The scale bars in Fig. 3 (a, c) represent a length of 100 nm. As compared to pure Ni–P coatings, the surface topography of composite coatings is different with lower degree of surface roughness and appearance of large clusters. Despite small quantities of nanostructures used, some degree

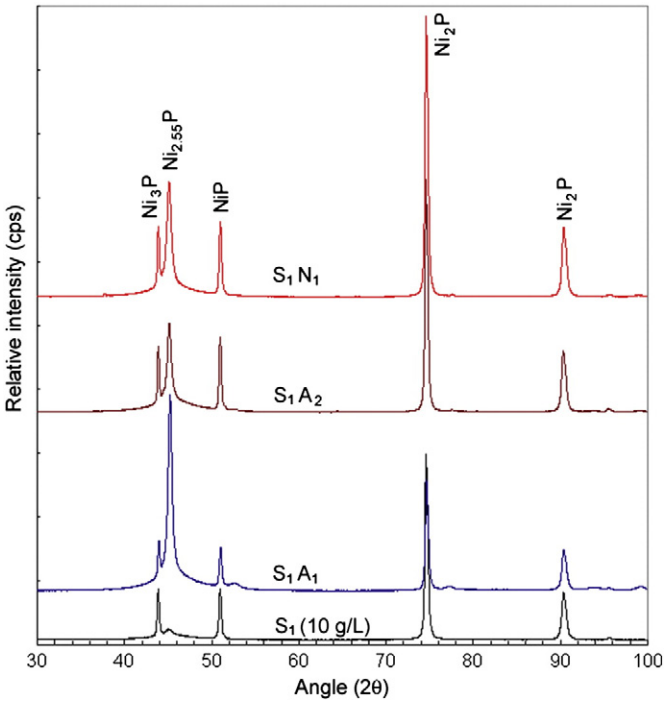

Fig. 2. X-ray diffraction patterns of the pure (S_1) and composite (S_1A_1, S_1A_2, S_1N_1) Ni–P coatings.

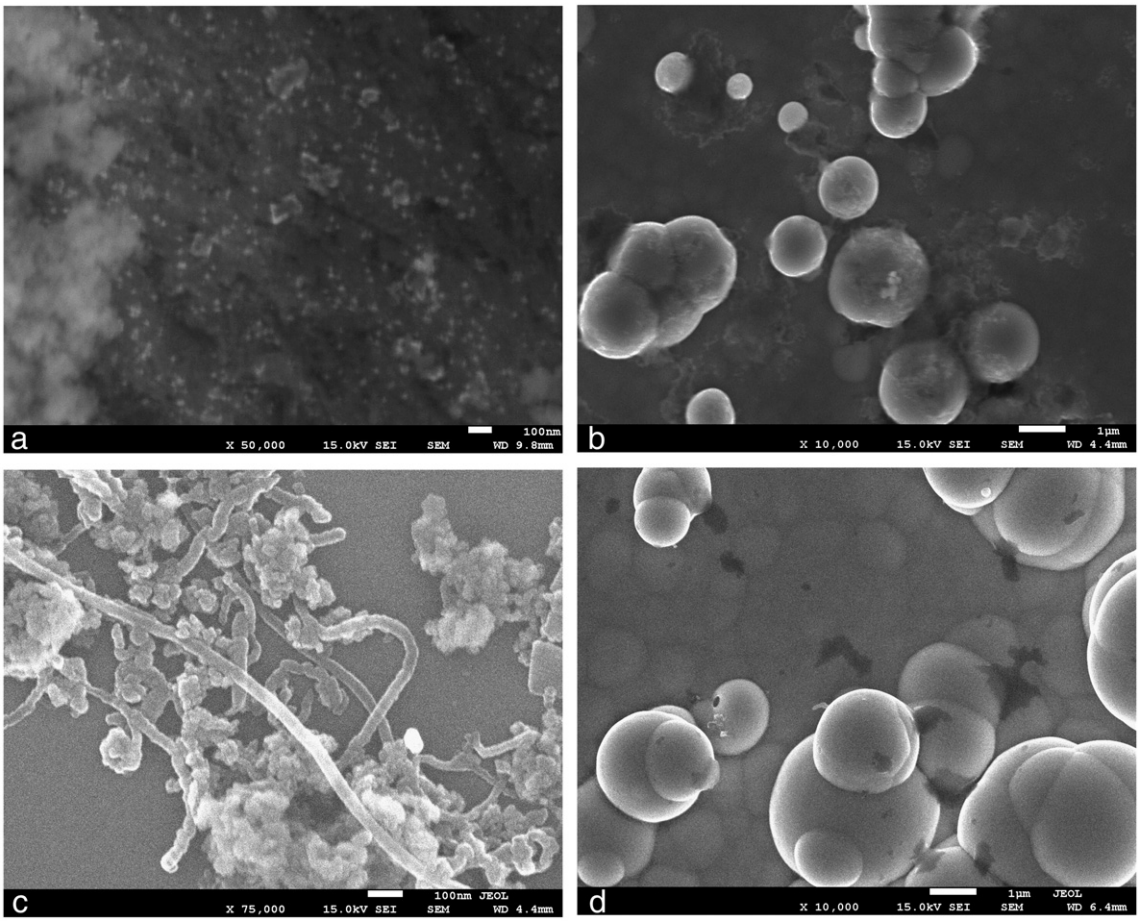

Fig. 3. FE-SEM microstructures of (a) Al_2O_3 nanoparticles, (b) Ni–P–Al_2O_3 composite coating (S_1A_1), (c) as-received multi-walled carbon nanotubes (CNT) and (d) Ni–P–CNT composite coating (S_1N_1).

of aggregation of these nanostructures might have occurred as evident in Fig. 3b. The addition of Al_2O_3 or CNT results in a more compact, dense deposit with no surface porosity or cracks as seen earlier in pure Ni–P coatings. Since incorporation of second phase into growing Ni–P matrix coating is primarily via physical adsorption, more intense agitation is needed to ensure continuous supply of nanostructures at the coating growth front. Also, the deposition rate drops during co-deposition, an observation that is consistent with earlier reports [26].

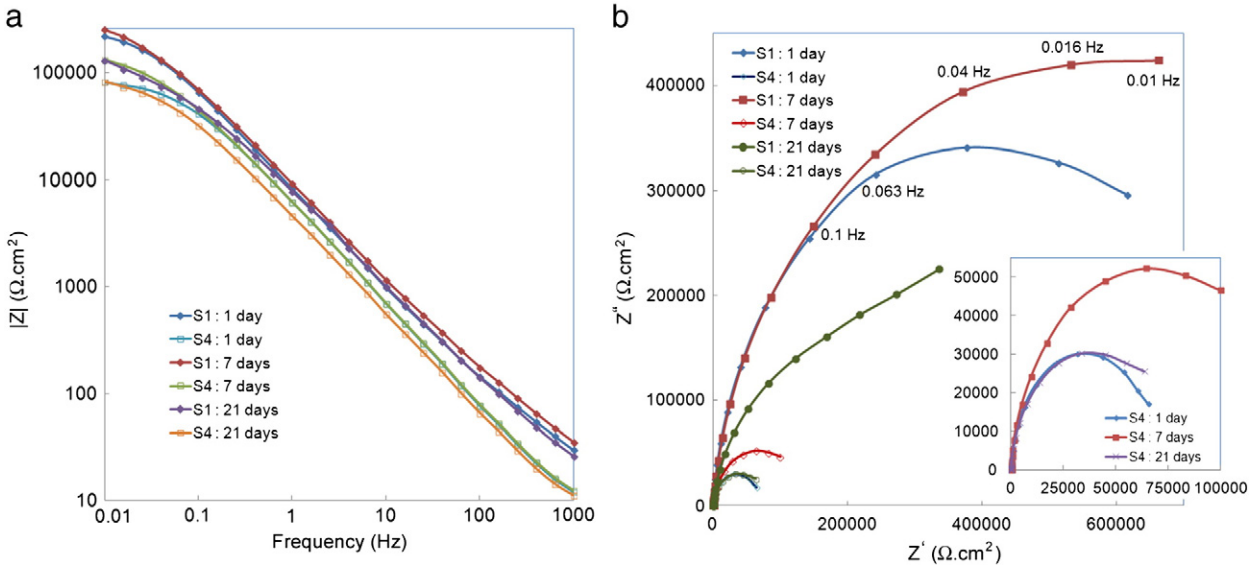

Fig. 4. EIS data for samples S_1 and S_4 upon immersion in 4 wt.% NaCl solution for 1, 7, and 21 days: (a) Bode diagram and (b) Nyquist plot. The inset in (b) gives enlarged view of Nyquist plot for S_4.

3.2. Corrosion properties

Electrochemical impedance spectroscopy (EIS) studies were performed on pure and composite coating samples in 4 wt.% NaCl salt solution. For pure Ni–P coatings (S1 and S4), Bode diagram (Log |Z| vs log f) and Nyquist plot for different immersion times are presented in Fig. 4. From comparison of S_1 and S_4 Bode plots, it is evident that S_1 offers superior resistance to corrosion at all immersion times. In both cases, however, the area impedance at low frequency (10 mHz) decreases with time and evidences the degradation of the coating in contact with the saline solution. As shown in Fig. 4b, Nyquist plots for both samples present a resistive loop after one day of immersion. For sample S_1, area impedance values at low frequency ($0.01 \leq f \leq 0.1$ Hz) are between 0.5 and 1.5 MΩ·cm^2 and are ten times higher than sample S_4. In addition, sample S_1 is more stable in the electrolyte with impedance at 10 mHz about 1.3 MΩ·cm^2 whereas the area impedance of sample S_4 decreases progressively below 0.1 MΩ·cm^2.

The superior corrosion resistance of the S_1 coating over S_4 was also confirmed from FE-SEM examination of the coatings after immersion in 4 wt.% NaCl for 42 days, as shown in Fig. 5. It is noticed that S_1 appears smooth, virtually crack-free and less damaged with formation of fine porous structure at some places (upper left corner of Fig. 5a). The sample S_4 underwent cracking throughout its surface along with presence of fine precipitates (inset of Fig. 5b). In the latter case, the cracks are ~180 nm wide and are interlinked such that the entire coating surface is divided into small fragments with each having size of the order of smaller than 10 μm.

Comparison of corrosion behavior for Ni–P–Al_2O_3 composite coatings in terms of Nyquist plots for samples S_1A_1 and S_1A_2 is made in Fig. 6. For Ni–P–Al_2O_3 coatings, the maximum area impedance value is of the order of ~10^4 Ω·cm^2 or less depending on immersion time and Al_2O_3 content. For all immersion times, the sample S_1A_2 exhibits higher area impedance values than those of S_1A_1 at low and intermediate frequencies. The data series with filled markers represent corrosion behavior of S_1A_1 coating. For sample S_1A_2, the area impedance value is maximum for fresh sample (i.e. immediately after immersion in salt solution) and then progressively drops for longer immersion times. The same trend follows in case of the S_1A_1 sample with similar behavior for 5 and 22 days immersion times. The real (Z') and imaginary (Z'') components of area impedance at 10 mHz and 0.1 Hz frequencies are indicated by arrows. Corrosion properties have been reported to improve [27] or deteriorate [28] upon incorporation of Al_2O_3 nanoparticles depending on its content in the bath. As opposed to earlier reports, however, the quantity of Al_2O_3 nanoparticles is very small (0.25 or 1.0 g/L) in our case and, as stated earlier, shows improvement in corrosion resistance upon increasing the Al_2O_3 content.

The EIS data for samples S_1C_1, S_4C_2 and S_1N_1 are shown in Fig. 7, with data series for samples S_1C_1 and S_4C_2 represented by filled and unfilled markers, respectively. All samples present resistive loop after one day of immersion and have similar low frequency area impedance between 2 and 4×10^4 Ω·cm^2. The sample S_1C_1 offers the best corrosion properties among the three types of composite coatings with similar Nyquist plots for immersion times of 1 and 5 days. After 22 days immersion, the maximum area impedance drops by a factor of 2, indicating lower corrosion resistance. The sample S_4C_2 has the lowest area impedance after 5 days of immersion with faster degradation in the electrolyte with low area impedance below 10^4 Ω·cm^2.

The adverse effect of porosity on corrosion behavior of protective coatings cannot be overlooked. Walsh et al. [29] performed an extensive review of both qualitative and quantitative measurement techniques for determination of porosity in electroless Ni–P coatings. In the absence of experimental data from other electrochemical porosity tests, a

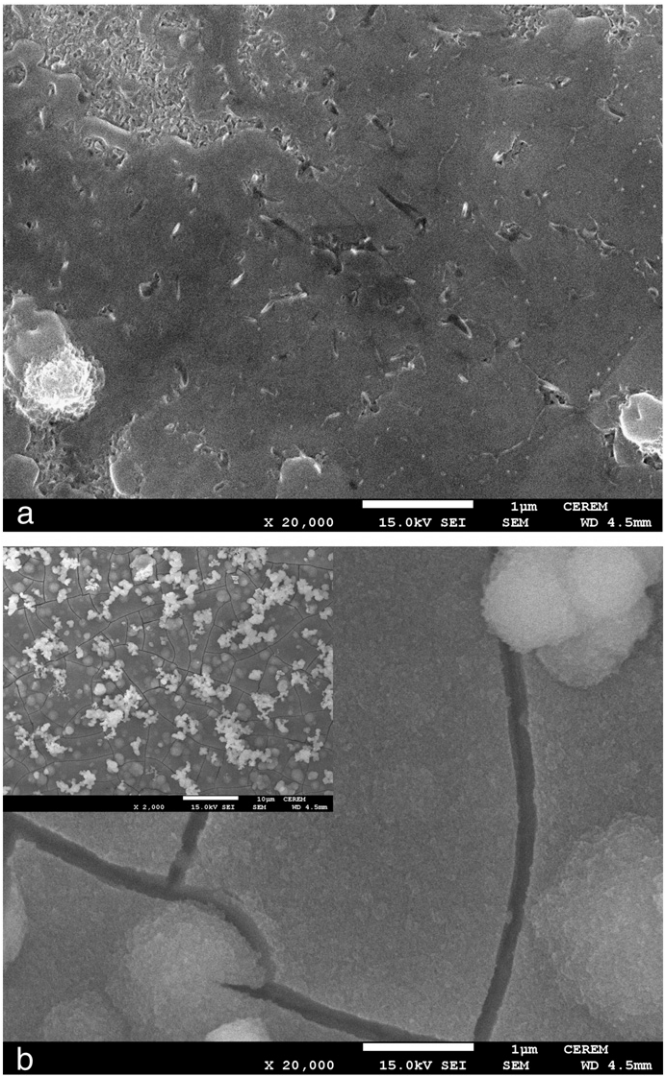

Fig. 5. FE-SEM micrographs of the (a) S_1 and (b) S_4 coating surfaces after immersion in 4 wt.% NaCl solution for 42 days. The inset in (b) is a low magnification image of the coating surface with scale bar representing a length of 10 μm.

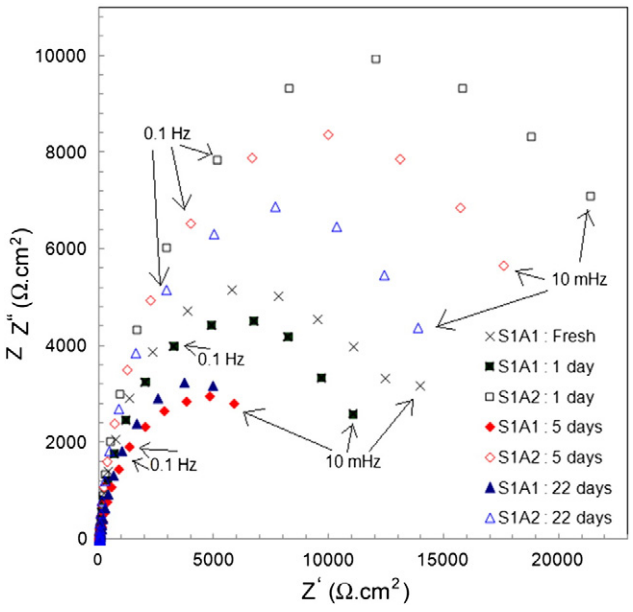

Fig. 6. Nyquist plot for up to 5 days of immersion 4 wt.% NaCl solution: (a) S_1A_1 and (b) S_1A_2.

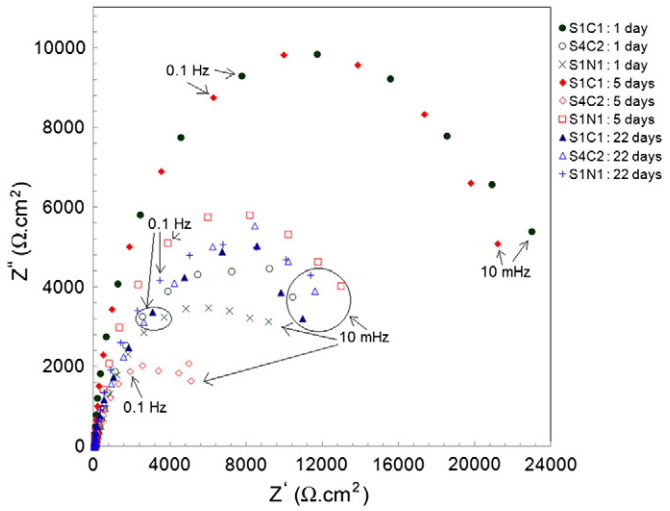

Fig. 7. Nyquist plot for S_1C_1, S_4C_2, and S_1N_1 composite coatings after different immersion times in 4 wt.% NaCl solution.

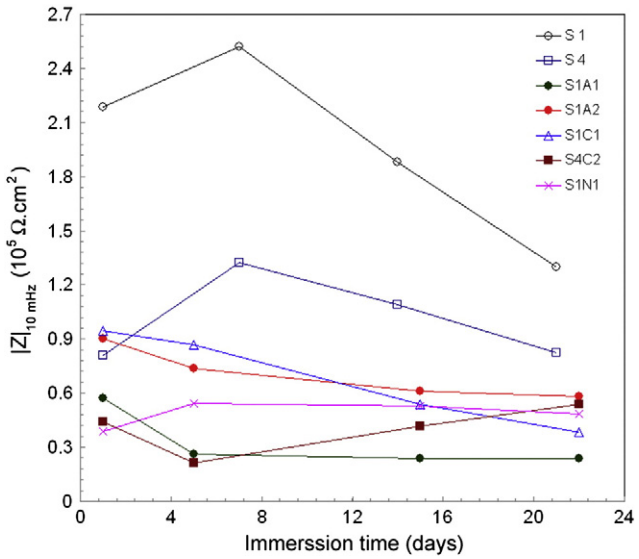

Fig. 8. Evolution of impedance at low frequency versus immersion time in 4% NaCl solution.

qualitative assessment regarding presence of pores in the pure and nanocomposite coatings is possible by means of a closer look at the results presented in this paper. In pure Ni–P coatings (S_1 and S_4), although presence of fine pores in the S_4 sample surface (Fig. 1d) leads to inferior degree of coating protection against corrosion in salt solution as manifested by cracking after prolonged exposure (Fig. 5b), Nyquist plots for both compositions nevertheless show one time constant. Since it is very hard for the electrolyte to penetrate through very fine pores, the shape of the Nyquist plot depends on the pore radius and length that in turn, are referred to as penetration depth (r) and pore length (l), respectively. The shape of the Nyquist plots obtained in our case is a semi-circle is similar to that predicted by the limiting case when $r \gg l$ and the ac signal manages to reach the bottom of the pore [30]. In such cases, the entire electrode behaves as a flat surface. Presence of a second phase as in case of nanocomposite coatings, in the form of dispersed nanoparticles up to a certain upper limit, has been reported to inhibit defect corrosion through their pore-filling action and by acting as a physical barrier to localized corrosion [31].

The summary of the evolution of area impedance at low frequency (10 mHz) for each coating at different immersion time in 4% NaCl solution is depicted in Fig. 8. The values of area impedance are between 2.5×10^4 and $2.5 \times 10^5\ \Omega \cdot cm^2$ and decrease with time attesting a progressive degradation of coatings except for the sample S_1N_1. The area impedance for the sample S_1N_1 increases with time but is still below samples without nanocomposites additives (Al_2O_3, SiC and CNT). Sample S_1 has the best corrosion resistance followed by sample S_4 with impedances about 1.8×10^5 and $0.75 \times 10^5\ \Omega \cdot cm^2$ respectively. Samples with nanocomposites additives have lower area impedance at the beginning of the test and after 9 days of immersion with area impedance below $10^5\ \Omega \cdot cm^2$.

3.3. Hardness values

Indentation of the pure Ni–P and Ni–P–SiC composite coatings provided insight into any change in coating hardness upon incorporation of nanostructures. For each coating composition, the hardness values were plotted to indicate scatter in data, as shown in Fig. 9. All the samples show higher levels of hardness than the copper substrate (1.80 GPa). For pure Ni–P coatings with different P content, the average hardness values were 7.4 and 4.4 GPa, respectively. Thus, an increase in P content from 8.5 (S_1) to 12.4 wt.% (S_4) caused drop in the overall coating hardness. Addition of as little as 0.25 g/L SiC nanoparticles in the plating bath and their subsequent incorporation into the coating resulted in average hardness of ~8.5 GPa, an increase by 14.0%. On the other hand, SiC addition to S_4 coating composition at similar loading level leads to a decrease in average hardness value. This observation is probably due to the combined adverse effect of higher porosity level and inhomogeneous distribution of SiC nanoparticles in the Ni–P coating matrix. Further experimentation is required to arrive at a concrete conclusion in this regard.

4. Conclusions

The change in electroless bath chemistry in terms of reducing agent content influences the final coating composition. An increase in RA amount from 10 to 25 m/L causes P content in the coating to increase from 8.5 to 12.4 wt.%. In addition to that, the coating surface morphology changes from rough with pores and cracks to dense, smoother with sub-micron size pores at the boundaries of round nodular structure.

EIS studies in 4 wt.% NaCl solution indicated superior corrosion resistance of medium P coatings with an area impedance value that is almost

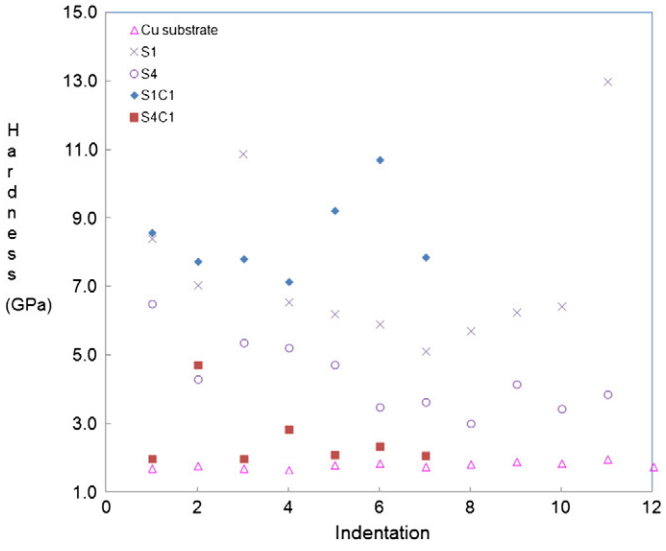

Fig. 9. Hardness data for pure Ni–P and some of the composite coatings.

10 times higher than that of high P coating. Incorporation of second phase nanostructures causes a decrease in coating growth rate and resistance to corrosion compared with pure Ni–P coatings. Among all the composite coatings with different loading levels, Ni–P–Al_2O_3 and Ni–P–SiC offer superior performance attributes than others, while Ni–P–CNT coating shows no structural degradation after several days of immersion in NaCl solution.

The results on nanoindentation show a gradual increase in average hardness value from the copper substrate (1.8 GPa) to medium-P coating (7.4 GPa) to Ni–P–SiC (8.5 GPa) indicating the effectiveness of hard nanoparticles towards improvement in hardness.

References

[1] W. Sha, X. Wu, K.G. Keong, Electroless Copper and Nickel–Phosphorus Plating: Processing, Characterization and Modeling, Woodhead Publishing Limited, Oxford, 2011.
[2] C.T.J. Low, R.G.A. Wills, F.C. Walsh, Surf. Coat. Technol. 201 (2006) 371.
[3] R. Parkinson, NiDI Tech. Ser. (1993) 22.
[4] J. Sudagar, J. Lian, W. Sha, J. Alloys Compd. 571 (2013) 183.
[5] F.B. Bahaaideen, Z.M. Ripin, Z.A. Ahmad, J. Sci. Ind. Res. 69 (2010) 830.
[6] W.X. Chen, J.P. Tu, H.Y. Gan, Z.D. Xu, Q.G. Wang, J.Y. Lee, Z.L. Liu, X.B. Zhang, Surf. Coat. Technol. 160 (2002) 68.
[7] S. Alirezaei, S.M. Monirvaghefi, M. Salehi, A. Saatchi, Wear 262 (2007) 978.
[8] J.N. Balaraju, Kalavati, K.S. Rajam, Surf. Coat. Technol. 200 (12-13) (2006) 3933.
[9] A.S. Hamdy, M.A. Shoeib, H. Hady, O.F.A. Salam, Surf. Coat. Technol. 202 (1) (2007) 162.
[10] A. Araghi, M.H. Paydar, Mater. Des. 31 (2010) 3095.
[11] O.A. León, M.H. Staia, H.E. Hintermann, Surf. Coat. Technol. 200 (5-6) (2005) 1825.
[12] A. Grosjean, M. Rezrazi, J. Takadoum, P. Bercot, Surf. Coat. Technol. 137 (1) (2001) 92.
[13] C.J. Lin, K.C. Chen, J.L. He, Wear 261 (2006) 1390.
[14] S. Zhang, K. Han, L. Cheng, Surf. Coat. Technol. 202 (2008) 2807.
[15] A. Farzaneh, M. Mohammadi, M. Ehteshamzadeh, F. Mohammadi, Appl. Surf. Sci. 276 (2013) 697.
[16] Y. de Hazan, D. Zimmermann, M. Z'graggen, S. Roos, C. Aneziris, H. Bollier, P. Fehr, T. Graule, Surf. Coat. Technol. 204 (2010) 3464.
[17] W. Chen, W. Gao, Y. He, Surf. Coat. Technol. 204 (2010) 2493.
[18] J. Novakovic, P. Vassiliou, Electrochim. Acta 54 (2009) 2499.
[19] B. Szczygieł, A. Turkiewicz, J. Serafińczuk, Surf. Coat. Technol. 202 (2008) 1904.
[20] A. Zarebidaki, S.-R. Allahkaram, J. Alloy Comp. 509 (2011) 1836.
[21] L.Y. Wang, J.P. Tu, W.X. Chen, Y.C. Wang, X.K. Liu, C. Olk, D.H. Cheng, X.B. Zhang, Wear 254 (2003) 1289.
[22] A.H. Graham, R.W. Lindsay, H.J. Read, J. Electrochem. Soc. 112 (4) (1965) 401–412.
[23] R. Elansezhian, B. Ramamoorthy, P.K. Nair, Surf. Coat. Technol. 203 (2008) 709.
[24] M. Islam, T. Shehbaz, Surf. Coat. Technol. 205 (2011) 4397.
[25] M. Islam, O.T. Inal, J.R. Luke, J. Appl. Phys. 100 (2006) 084903.
[26] I.R. Mafi, C. Dehghanian, Appl. Surf. Sci. 257 (2011) 8653.
[27] A.S. Hamdy, M.A. Shoeib, H. Hady, Mater. Lett. 80 (2012) 191.
[28] C. Li, Y. Wang, Z. Pan, Mater. Des. 47 (2013) 443.
[29] F.C. Walsh, C.P. de León, C. Kerr, S. Court, B.D. Barker, Surf. Coat. Technol. 202 (2008) 5092.
[30] A. Lasia, in: B.E. Conway, J. Bockris, R.E. White (Eds.), Modern Aspects of Electrochemistry, Vol. 32, Kluwer Academic/Plenum Publishers, New York, 1999, pp. 143–248.
[31] H.A. Sorkhabi, M. Esohagh, Corros. Sci. (2013), http://dx.doi.org/10.1016/j.corsci.2013.07.046.